2025 IEEE International Conference on Robotics and Automation (ICRA 2025)
May 19-23, 2025. Atlanta, USA

Strain-Coordinated Formation, Migration, and Encapsulation Behaviors in a Tethered Robot Collective

Sadie Cutler[1], Danna Ma[2], and Kirstin Petersen[2]

***Abstract*— Tethers are an underutilized tool in multi-robot systems: tethers can provide power, facilitate retrieval and sensing, and be used to manipulate and gather objects. Starting with the simplest possible configuration, our work explores how agents linked in series by flexible, passive, fixed-length tethers, can use those tethers as sensors to achieve distributed formation control. In this study, we extend upon previous work to show the applicability of strain-coordinated formation control for encapsulation and migration along a global gradient as well as the trade-offs between formation control and taxis in an obstacle-laden environment. Our results indicate significant potential for tethered robot collectives: versatile behaviors that can work on simple, resource-constrained robots or serve as a fallback mechanism in case more sophisticated means of coordination fail.**

I. Introduction

Multi-robot systems are more robust to individual failures, adapt better to changing circumstances and tasks, and are capable of monitoring larger areas than their single counterparts. It can be challenging, however, to ensure multi-robot systems coordinate efficiently in scenarios where robot hardware is constrained by volume, payload, power, or cost (e.g. mm-μm-scale robots [1], [2]), or where the environment they work in is dynamic, communication-restricted, or visibility-limited (e.g. underground, deep sea, or military applications [3]).

Tethers, taut and loose, have been used in robotics to provide power and stabilization [4], ensure recoverability [5], [6], assist with object capture [7], [8], and aid construction [9], [10]. In this work, we demonstrate expanded capabilities of tether-based coordination in multi-robot systems which operate without the use of communication or long-range exteroceptive sensors – making these collectives ideal for communication-restricted and/or visibility-limited environments. Our previous work demonstrated that proprioceptive sensing of tethers could be used by agents to navigate relative to their connected neighbors, enabling the collective to transition between formations.

Our algorithm, originally proposed in [11], is completely distributed and reactive; it does not require global planning, inter-agent communication, or for agents to know or sense the current or desired state of any other agent. Specifically, in [11] we investigated teams of 5-35 simulated agents connected in series by fixed-length, passive tethers. Robots were able to transition successfully between a large range of formations in two dimensions using proprioceptive sensing of tether strain and angle, along with close-range sensors for avoiding collisions with other agents.

In this paper, we further that work by presenting: 1) algorithm extensions to enable taxis toward a global source of attraction, 2) investigation of trade-offs between taxis and formation control in obstacle-laden environments, and 3) use of tethered collective to seek and encapsulate a target.

Sec. II, discusses the general use of tethers in robotic systems. Secs. III-IV provides a review of the simulation framework, algorithm, and approach, along with the introduction of a new objective vector for taxis. The new strain-coordinated behavior of taxis in an obstacle-laden environment is shown in Sec. V and the trade-off between taxis and maintaining formation is analyzed. Sec. VI demonstrates the use of trade-offs between taxis and formation control for encapsulation. Sec. VII covers implications and future directions. This work helps pave the way for coordinated behaviors in simple, resource-constrained multi-robot systems.

II. Related Work

Tethers have been used for many purposes in ground, water, aerial, and space robotics, and fall into two main use cases: 1) tethers providing support, e.g. power delivery, wired communication, recoverability, and material delivery for construction [10], [4], [5], [9], [12]; and 2) tethers adding primary functionality, such as improving robot stability or enabling robots to tow, contain, capture, or sort objects [8], [13], [14], [7], [15], [16], [17], [6]. The former category typically involves loose tethers, whereas tethers in the latter category may be either loose or taut.

Our original algorithm [11] utilizes the tether solely for support, constraining the tether to be taut and using the tension and relative angle of the tether to estimate the position of each robot relative to its neighbors by applying distance- and bearing-based control [18], [19]. This concept has been demonstrated previously by others in simulation and with limited hardware for single quadcopters using both fixed- [20] and variable-length tethers [21]. Unlike the previous work of others, however, our robots rely on position and strain in their tethers to estimate distance and bearing to their connected neighbors which informs a cohesive control strategy [11], without the need to synchronize or elect a leader.

This work was funded by a Packard Fellowship for Science and Engineering and NSF #2042411.

[2]School of Electrical and Computer Engineering, Cornell University, Ithaca, NY 14853, USA kirstin@cornell.edu

[1]Sibley School of Mechanical and Aerospace Engineering, Cornell University, Ithaca, NY 14853, USA sc3236@cornell.edu

Our original work presented an algorithm to enable transitions between multi-robot formations. In this paper, to make such capabilities more practically useful, we extend the algorithm to incorporate taxis such that we can produce goal-oriented migration of formations as well as encapsulation behaviors. Furthermore, taking into consideration operation in cluttered environments, we investigate the risk of entrapment posed by formation shape, orientation, and desire to maintain formation versus making progress toward the goal. While taxis and encapsulation are both well-explored in the field of robotics, their implementation with our sensing-limited and communication-denied tethered agents is significant. In addition, this extended algorithm is the first to make dual use of the tethers: for support (localization) and for primary functionality (encapsulation).

III. Simulation Framework

We designed a simulation framework in which N homogeneous, mobile agents of diameter $D = 5$ move on a plane. Agents move asynchronously and are connected in series by equal-length, flexible tethers which can rotate freely around the center point of each agent. For the purposes of this paper, we assume agents cannot drag their neighbors out of place. Each tether has a measured length l and nominal length $l_o = 5D$, and a measured strain $\varepsilon = \frac{l}{l_o}$ and nominal strain $\varepsilon_o = 1$. As shown in Fig. 1, when the tethers are taut the agents can measure their angle, θ, with respect to their heading. The angle between the two tethers is defined as $\delta = \theta_- + \theta_+$. Additionally, our model assumes that agents are capable of perceiving distance and bearing to obstacles including other agents and tethers that are closer than D to the agent's center, similar to IR sensors on the periphery of the robot. To achieve multi-agent formation control, formations are specified as a set of relative goal angles, δ_o, between an agent's two tethers. To navigate, agents compare the goal angle, δ_o, to the measured angle, δ, by computing $\delta_e = \delta_o - \delta$.

Our simulation assumes that agents can perform taxis using a local gradient; agents tune the relative importance of their objectives to reach the goal while maintaining formation. To quantify agents' success in maintaining formation and progressing toward a goal, the following measures are computed for analysis: the sum of angle errors in the formations $\sum_2^{N-1} \frac{\delta_e}{\delta_o}$, the normalized distance traveled to the goal $\frac{d_t}{d_o}$ (where d_t is the distance traveled by the central agent and d_o is its straight-line distance from the start to the goal with no obstacles), and the measured strain ε.

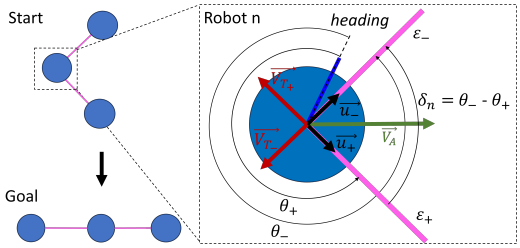

Fig. 1: Tethered collective of 3 agents, and its start and goal formations. The blow-out shows the information available to the central agent: current angle (θ) and strain (ε) of the trailing ($-$) and leading ($+$) tethers measured in the reference frame of the agent. The agent uses this information to create: the unit vector for tether strain u, the force/direction required to maintain ε_o shown as $\overrightarrow{V_T}$, and the force/direction required to reduce $\delta_e = \delta_o - \delta$ shown as $\overrightarrow{V_A}$ (see Sec. IV for vector definitions).

IV. Distributed Coordination

The coordination algorithm aims to: 1) reach δ_o, 2) maintain l_o, 3) avoid collisions with any other agents or tethers, and, if present, 4) perform taxis on a global gradient. In every time step, an agent senses its proximity to the goal and the angle and strain of its tethers. It then computes δ_e and the objective vectors and uses this information to take a step. Similar to real hardware, agents have a maximum velocity set to 2.5 (units/time step); this further helps ensure recoverable changes to l. Agents are updated in random order in every time step to mimic asynchrony. The policy described below is distributed and enforced on each agent, independent of what other agents are experiencing. What follows is a brief description of how an agent computes each objective vector.

A. Objective 1: Angle Difference

The objective $\overrightarrow{V_A}$ decreases the error in the relative angle between the tethers, δ_e; the magnitude of $\overrightarrow{V_A}$ is proportional to the amplitude of the error. The agent aligns its heading to the center of the two tethers (Fig. 1), and drives either toward the heading to increase δ, or away from the heading to decrease δ as dictated by the sign of δ_e. Agents at the end of the configuration have only one tether and are not influenced by this objective.

$$\overrightarrow{V_A} = sign(\delta_o - \delta)\sqrt{\frac{|\delta_o - \delta|}{2\pi}}\frac{\overrightarrow{u}_- + \overrightarrow{u}_+}{|\overrightarrow{u}_- + \overrightarrow{u}_+|} \quad (1)$$

where $\overrightarrow{u}_-$ and $\overrightarrow{u}_+$ are unit vectors pointing toward the tethered neighbors and $sign$ returns +1, 0, or -1 depending on the sign of the error, δ_e.

B. Objective 2: Tether Tautness

Since θ and ε are only deemed accurate when the tether is taut ($l = \pm.1l_o$), the objective $\overrightarrow{V_T}$ aims to maintain l_o (Fig. 1). The agent drives along $\overrightarrow{u}$, away from a neighboring agent, if $l < l_o$, or toward the neighboring agent if $l > l_o$.

$$\overrightarrow{V_T} = sign(\varepsilon - \varepsilon_o)(\varepsilon - \varepsilon_o)^2\overrightarrow{u} \quad (2)$$

where ε and $\overrightarrow{u}$ correspond to ε_+ and $\overrightarrow{u}_+$, or ε_- and $\overrightarrow{u}_-$ depending on whether the tether is connected to the leading or trailing agent, respectively. How $|\overrightarrow{V_T}|$ changes with the length of the tether is shown in Fig. 2, which resembles a typical hyperelastic stress-strain curve.

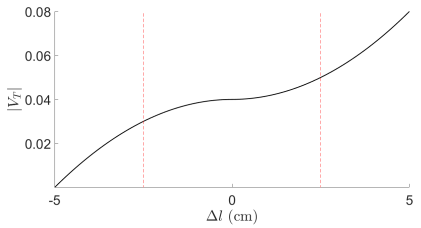

Fig. 2: Effect of changes in tether length on objective vector, $\overrightarrow{V_T}$.

C. Objective 3: Repulsion for Collision Avoidance

In our prior work, agents were only capable of sensing other agents which led to frequent entanglements. Here, we assume that agents are capable of sensing other agents and non-adjacent tethers, using e.g. IR or ToF sensors, to prevent collisions and tether entanglement. Furthermore, we assume they can distinguish between agents/tethers and passive obstacles. The objective, $\overrightarrow{V_R}$ directs the agent to move away from the nearest collision point.

$$\overrightarrow{V_R} = 8De^{-\frac{d^2}{2(D/2)^2}}\overrightarrow{\mathrm{u}}_R \tag{3}$$

This gives us a Gaussian curve with $\sigma = D/2$ and amplitude = $8D$, where the unit vector $\overrightarrow{\mathrm{u}}_R$, with a distance d, points from the center of the agent to the nearest point on the perceived agent/tether. The agents will bypass rather than actively avoid stationary obstacles.

D. Objective 4: Global Attraction

The objective, $\overrightarrow{V_G}$ incentivizes an agent to follow a 2D global gradient toward a goal. This is accomplished by adding a global point of attraction, such as a light source, which dictates $\overrightarrow{V_G}$:

$$\overrightarrow{V_G} = G\overrightarrow{\mathrm{u}}_{V_G}; \tag{4}$$

where G is treated as a piece-wise linear function. When the Euclidean distance from the agent to the goal, d_e, is large and the angle error is small, we increase G to prioritize progress, permitting formation distortion and rotation to bypass obstacles. When the distance to the goal is small or the angle error is large, we decrease G to prioritize maintaining formation over making progress toward the goal.

$$G = \begin{cases} 1 & (\delta_e \leq \pm 5°, d_e > 8l_o) \\ 0.1 & (\delta_e > \pm 5°, d_e > 8l_o) \\ 0.1 & (\delta_e \leq \pm 5°, d_e \leq 8l_o) \end{cases} \tag{5}$$

E. Resultant Vector

The resultant vector $\overrightarrow{V}$ is the scaled sum of all the objective vectors described above and determines an agent's velocity in the current step.

$$\overrightarrow{V} = c_A\overrightarrow{V_A} + c_T(\overrightarrow{V}_{T_-} + \overrightarrow{V}_{T_+}) + \overrightarrow{V}_R + c_G\overrightarrow{V}_G \tag{6}$$

where, by design, c_T is the largest scaling factor to ensure the tethers stay taut, c_A is second largest, and c_G is the smallest. In the following experiments, c_T was set to 300. The following section discusses how to trade off the other objectives so that the agent prioritizes either maintaining formation or taxis depending on the task and environment.

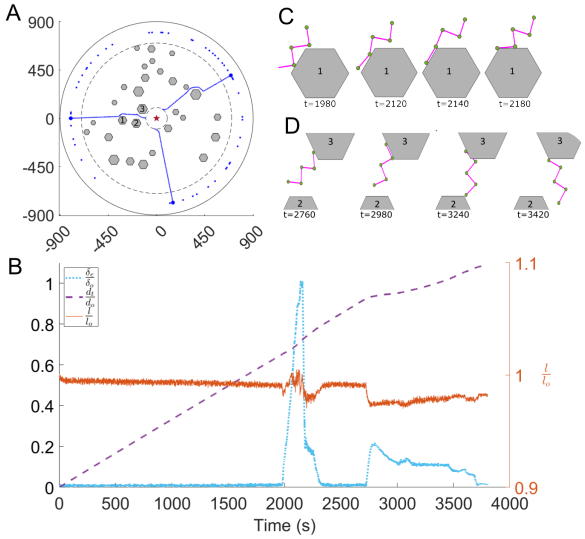

Fig. 3: A) A cluttered environment used for analysis with 50 random starting locations (green dots in the outer circle), the goal location (central red star), and three example runs (with the path of the central agent in the collective marked in blue), B) Plot of δ_e, d_t, and l over time for the left-most path shown in (A). Insets (C) and (D) show shape distortion and rotation, respectively, resulting from the collective's interaction with obstacles 1-3 in (A).

V. Taxis and Formation Control

In the presence of a global gradient and the absence of obstacles, the collective moves in formation toward a goal. When navigating narrow or cluttered spaces, three behaviors emerge: 1) the shape of the collective distorts to bypass an obstacle, 2) the collective rotates to bypass an obstacle, or 3) competing objective vectors prevent the collective from progressing toward the goal until scaling factors are changed. We first analyze the effect of relative scaling factors, then use these to inform optimal scaling and further test the impact of starting orientation and formations in a simulated, cluttered test environment.

A circular environment of diameter 1800 with 29 obstacles of random size and position was generated, leaving the space around the starting perimeter and goal perimeter clear. The obstacles were all hexagonal with a maximum diameter randomly chosen between 40-100. A collective starts in the desired formation at one of 50 randomly-selected positions on the edge (Fig. 3A). A "W"-formation was used as the default formation for testing starting orientation and scaling factors; when testing the effects of formation, random formations were generated.

Fig. 3B shows the first two behaviors of the collective (as discussed above) when encountering an obstacle in its path. In the first, the formation is partially distorted upon initial contact with obstacle 1 (Fig. 3C); in this case δ_e increases which results in more strain on the tethers and the δ_o is recovered shortly after passing obstacle 1. Later, when the collective encounters obstacles 2-3, the formation rotates (Fig. 3D) which temporarily results in a smaller increase in δ_e, a slightly larger increase in d_t, and a slight decrease in

ε.

A. Evaluation

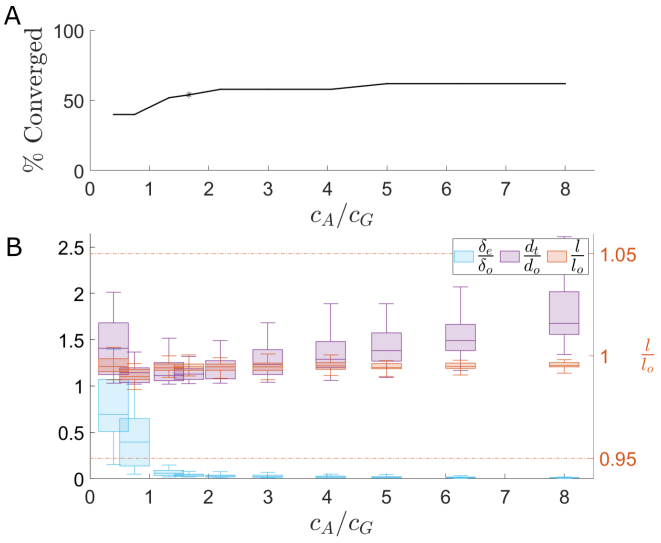

Fig. 4: The effects of the relative scaling of c_A to c_G on: A) the ability of collectives to converge on the goal position & maintain formation and B) d_t, average δ_e and l. Red dotted lines indicate bounds on acceptable tether lengths. The '*' in (A) corresponds to the scaling factors used in the remaining simulations.

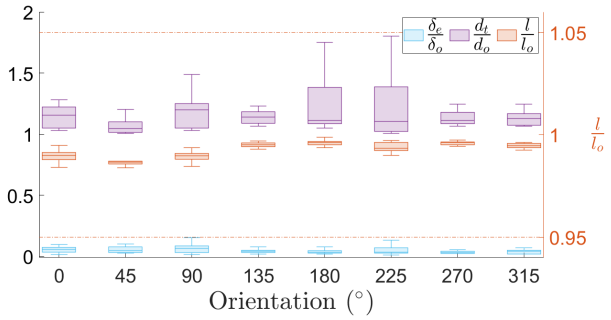

Fig. 5: The effects of orientation of the "W" formation relative to the goal on d_t and average δ_e and l. Red dotted lines indicate bounds on acceptable tether lengths.

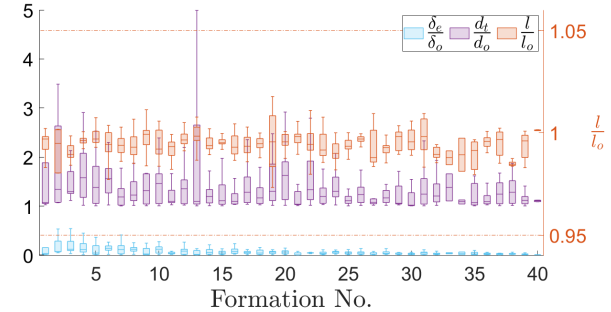

Fig. 6: The effects of formation shape on d_t and average δ_e and l, sorted according to δ_e. Red dotted lines indicate bounds on acceptable tether lengths.

Using the 50 different starting positions, we ran a parameter sweep of scaling factors to examine the system's dependence on angle vs tether strain objectives. Changing the factors c_A and c_G had a significant impact on both formation accuracy and distance traveled. As shown in Fig. 4B and the parameter sweeps in [11], there is a lenient range of values that yields good performance. Fig. 4 shows that at low values of $\frac{c_A}{c_G}$, δ_e is high because the high c_G attracts agents toward the goal more than c_A incentivizes them to maintain δ_o. At high values of $\frac{c_A}{c_G}$, i.e. where the primary incentive is to maintain formation, δ_e decreases while d_t increases because the collective covers additional distance trying to maneuver around obstacles. Tether length is fairly constant for all parameters. Based on these findings, all further simulations were performed with: $c_A = 2.5$ and $c_G = 1.5$ ($\frac{cA}{cG} = 1.7$)

Next we examined the effect of initial orientation (Fig. 5) and desired formation (6). The data plotted in these graphs represent the trials that converged on the global goal position while maintaining formation: 294/400 and 3820/5000, respectively.

Orientation has little effect on δ_e, d_t, or l; this is unsurprising as formations often rotate as a collective moves toward the goal, negating any advantage of a particular starting orientation. On average, the collective travels 1.21 times the d_o, keeps the tethers taut, and shows moderate δ_e. The desired formation, however, has a stronger effect on d_t and ε and much greater variation. Not all randomly-generated formations, especially those with the small angles and scrunched shape that characterized formations that failed, are likely to be practically useful.

B. Mitigating Stagnation to Increase Convergence

For those trials that failed to converge, this was almost exclusively due to the formation being stuck on an obstacle, i.e. competing objective vectors prevented the collective from progressing toward the goal. In Fig. 7, the formation encounters an obstacle around time step 800 and agents' velocities decrease as their resultant vectors (seen in overlaid images) are pointing toward the obstacle, halting forward progress. By time step 1400, the majority of the resultant vectors push directly into the object causing the formation

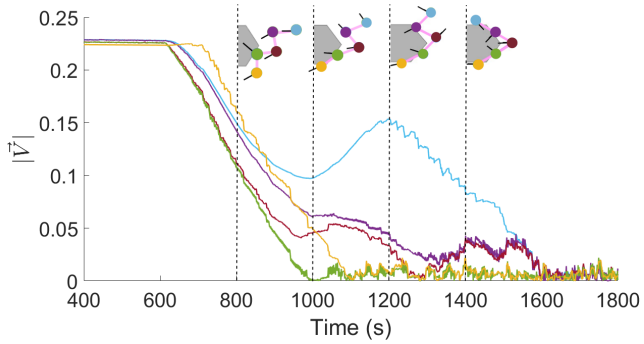

Fig. 7: $|\vec{V}|$ for 5 agents as they proceed toward the goal. Snapshots of the formation at four different time steps are overlaid with black lines indicating the direction of $\vec{V}$.

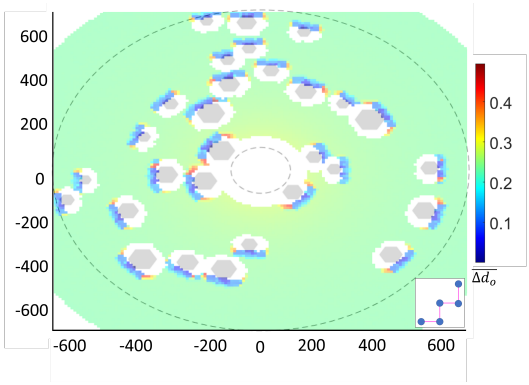

Fig. 8: Heat map of the mean velocity of the collective, starting at each of the cells in the heat map, and progressing toward the goal. The values of $\Delta\bar{d}_o$ are averaged over 50 time steps.

to stagnate i.e. agents do not return to δ_o or make progress toward the goal.

Fig. 8 depicts the collective's mean progress toward the goal (across 50 time steps), which is a reasonable approximation for the collective's aggregate resultant vectors. In each instance, the same starting point and configuration with respect to the target (shown in the inset of Fig. 8) were used. The collective maintains its nominal velocity (0.22/time step) when moving in free space; when the collective encounters obstacles, however, it slows down and can stagnate. Interestingly, if the formation deforms while bypassing an obstacle, the collective may briefly speed up to maintain separation between agents.

The problem of stagnation has a straightforward solution, as discussed in Sec. V-A: agents can monitor their individual progress by tracking how the distance to the goal changes. When Δd_o, averaged over 50 time steps, drops below a threshold (here 0.01), agents lower the priority of staying in formation by decreasing $c_A = \frac{1}{8}c_A$ and increasing $c_G = 8c_G$ to incentivize progress toward the goal, until the change in distance is above the threshold. With this modification, the number of completed cases for the effect of orientation (out of 400 trials) increased from 73.5% to 95.0%. Of the remaining unfinished cases, 1% were collisions between agents and tethers and 4% remained stuck on obstacles.

VI. Encapsulation

Taxis and formation control can also be extended to the task of encapsulation which adds a primary function for the tethers, in addition to their role as support for formation control. To perform this task, we assume that the object is broadcasting a stimulus, e.g. a light or heat signature, and that agents are able to sense the absolute value of that stimulus (the distance to the object is used as a proxy) which can help trigger new behaviors when certain thresholds are crossed. The challenge then is to enable many agents to coordinate encapsulation, despite only knowing the strain and bearing of the two tethers which connect them to their neighbors. To perform encapsulation, individual agents adjust their piece-wise incentives $(\overrightarrow{V_G}, \overrightarrow{V_A})$ based on the target

Algorithm 1 Algorithm for encapsulating a hexagon with a pinch formation. Each agent uses the entries corresponding to its location in the chain in the following lists:
$Role = [0, 1, 1, 1, 1, 2, 2, 2, 1, 1, 1, 1, 0]$,
$\delta_o = [-, \pi, \pi, \pi, \pi, \pi, \frac{\pi}{3}, \pi, \pi, \pi, \pi, \pi, -]$ (V-form.),
$\delta'_o = [-, \frac{3\pi}{4}, \pi, \frac{\pi}{2}, \pi, \pi, \frac{2\pi}{5}, \pi, \pi, \frac{\pi}{2}, \pi, \frac{3\pi}{4}, -]$ (Pinch-form.),
$T = [\infty, 1600, \infty, 1500, \infty, \infty, 1000, \infty, \infty, 1500, \infty, 1600, \infty]$ (timer threshold).

```
if d_e > 4l_o then
    if role = 0 then G ← 2/3
    else G ← 0
    end if
else
    t ← t + 1
    if t > t_thr then δ_o ← δ_{o,n}
    end if
    if d_e ≤ 3l_o and |δ − δ_o| < 5° then
        if role = 2 then
            G ← 0.1
        else
            G ← 0.01
        end if
    end if
end if
```

stimulus. We consider an object encapsulated if $\geq$ 80% of the object is covered by the collective's alpha shape (the smallest 2D area that comprises all the robots in the collective without any holes). To highlight some of the interesting and challenging aspects of encapsulation, we use more robots (13) than for the formation and migration tasks.

Our first approach was to incentivize encapsulation with a specified formation. To do this, each agent follows Alg. 1. Carefully timed behaviors allow some agents to get much closer than others to the target before the capture formation is triggered. In Fig.9 we show an example of a 13-agent collective encapsulating a hexagon of $area = .19A$, where A is the largest encapsulating area of a 13-agent collective, i.e. circle formation. This pinch-grip works well for targets of varied shapes as long as the $area \leq .19A$.

Encapsulation with a specific capture formation, however, requires careful customization of the number of agents and the size and shape of the object. If we are more lenient about how the object is encapsulated, we can leverage the trade-offs discussed in Sec. V-A to drastically simplify the algorithm, while achieving a behavior which is somewhat agnostic to the size/shape of the object it can encapsulate (Alg. 2). These simplifications prioritize the importance of the collective encapsulating the target over maintaining

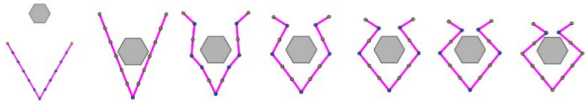

Fig. 9: The collective approaches and encapsulates a hexagon

Algorithm 2 Algorithm for encapsulating general objects.

if $d_e > 4l_o$ **then**
  if $role = 0$ **then** $G \leftarrow \frac{2}{3}$
  else $G \leftarrow 0$
  end if
else
  $G \leftarrow 0.05$, $c_A \leftarrow 0.7c_A$, $\delta_o \leftarrow \pi$
end if

formation. We know from our prior work [11] that the collective can transition from any random formation to a straight line. It follows therefore, that if a straight line can encapsulate a target, any other formation can as well. To this end, we used Alg. 2 with a straight line formation in seven different orientations, starting from 0°in 15°increments, to encapsulate four target shapes (hexagon, square, diamond, and triangle) with areas varying from $0.05A - .63A$. The results are shown in Fig. 10; the collective successfully captures objects of $area = 0.19A$ in 26/28 (92.9%) trials across the four shapes, and is similarly successful at encapsulating of targets up to ∼12 times larger than the pinch-grip.

In those cases that failed, the increase in $\overrightarrow{V_G}$ (that is activated near the target) acts co-linear to $\overrightarrow{V_T}$, overcoming it and resulting in a collision; this phenomena is especially prevalent when the straight line-formation starts aligned with x-axis (0°rotation).

For comparison, we also tested Alg. 2 with 50 randomly-generated formations. Starting from the same point, with random orientations, and with a hexagon of $area = .19A$, these randomly-generated formations successfully encapsulated the target in 21/50 (42%) trials (some examples of successful encapsulation are shown in Fig. 10C). Of the random cases that failed, 8 had collisions, and the remaining 21 had trouble balancing incentives (transitioning to the new formation and reaching the goal) – this was especially true for formations that started very scrunched.

Although the straight-line configuration was more successful at encapsulating targets, it is worth noting that even starting from a random, arbitrarily difficult starting formation the collective can encapsulate large objects utilizing a simple algorithm (Alg. 2). Additionally, straight-line formations with the line oriented to the y-axis and perpendicular to the target (rotated 90°) performed remarkably well, encapsulating 100% of hexagons at all tested sizes. This has exciting implications for reducing the number of agents with long-range stimuli sensing.

VII. Conclusion

In this paper, we build on previous work to expand the set of strain-coordinated behaviors for a tethered robot collective with no communication, minimal sensing, and distributed control to include taxis and encapsulation. This work investigates 1) the trade-offs between taxis and maintaining formation in an obstacle-laden environment, 2) how the relative desire to maintain formation versus reach the goal, and the starting orientation and formations affect convergence,

A

Area:	.05A	.13A	.19A	.27A	.42A	.49A	.56A	.63A
	7/7	7/7	7/7	7/7	7/7	6/7	7/7	7/7
	4/7	3/7	5/7	4/7	5/7	6/7	3/7	5/7
	3/7	4/7	4/7	5/7	2/7	7/7	4/7	4/7
	2/7	3/7	4/7	4/7	7/7	6/7	6/7	5/7

B

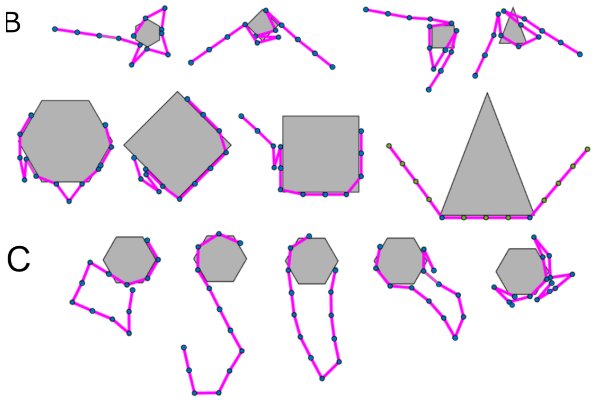

C

Fig. 10: A) Successful encapsulations of objects by area; B) Example final encapsulation for each shape of $area = .05A, .63A$. C) Example final encapsulations of a hexagon ($area = .19A$) with random starting formations. Note: our current simulator simplifies tethers to appear as straight lines, therefore they sometimes appear to overlap with objects.

and 3) the use of tethers to perform an encapsulation task, in addition to supporting relative localization functionality.

We found that, in terms of successful taxis to a designated goal area, there appears to be a lenient range where the related scaling factors yield consistent results. We determined that starting orientation matters little to the outcome, although some formations have a much easier time navigating past obstacles. Since, for example, heavily contorted formations are likely unsuitable for general robotic applications, we hypothesize that these problematic formations can be avoided or adjusted.

There are many exciting avenues for future work: 1) improving the capability of the simulator to include physics-based phenomena, such as robots dragging other robots, tethers bending around objects, or environments with varying motion resistance; 2) exploring the robustness of the algorithm to sensor and motion noise and resilience to robot heterogeneity; 3) improving encapsulation robustness; 4) expanding the capability of the algorithm to gather, separate, and encapsulate multiple non-fixed objects; 5) investigating the potential of collectives with more complicated tether configurations; and 6) implementing a test platform to validate these behaviors in real experiments.

These simple means for coordinating complex behaviors in robot collectives promise a wide range of applications for sensor-limited and communication-denied robots, and also as a fail-safe mode to support recovery in case other modalities fail on more sophisticated robots.

REFERENCES

[1] G. C. de Croon, J. Dupeyroux, S. B. Fuller, and J. A. Marshall, "Insect-inspired ai for autonomous robots," *Science robotics*, vol. 7, no. 67, p. eabl6334, 2022.

[2] E. Farrell Helbling and R. J. Wood, "A review of propulsion, power, and control architectures for insect-scale flapping-wing vehicles," *Applied Mechanics Reviews*, vol. 70, no. 1, p. 010801, 2018.

[3] C. Wong, E. Yang, X.-T. Yan, and D. Gu, "Autonomous robots for harsh environments: a holistic overview of current solutions and ongoing challenges," *Systems Science & Control Engineering*, vol. 6, no. 1, pp. 213–219, 2018.

[4] B. Kosarnovsky and S. Arogeti, "Geometric and constrained control for a string of tethered drones," *Robotics and Autonomous Systems*, vol. 133, p. 103609, 2020. [Online]. Available: https://www.sciencedirect.com/science/article/pii/S0921889020304498

[5] H. Sato, K. Uchiyama, F. Ito, R. Sawahashi, and T. Nakamura, "Distributed deployment with multiple moving robots for long distance complex pipe inspection," *IEEE Robotics and Automation Letters*, vol. 7, no. 4, pp. 11 252–11 259, 2022.

[6] S.-R. Oh, K. Pathak, S. K. Agrawal, H. R. Pota, and M. Garratt, "Approaches for a tether-guided landing of an autonomous helicopter," *IEEE Transactions on Robotics*, vol. 22, no. 3, pp. 536–544, 2006.

[7] F. Zhang, P. Huang, Z. Meng, Y. Zhang, and Z. Liu, "Dynamics analysis and controller design for maneuverable tethered space net robot," *Journal of guidance, control, and dynamics*, vol. 40, no. 11, pp. 2828–2843, 2017.

[8] Y. Su, Y. Jiang, Y. Zhu, and H. Liu, "Object gathering with a tethered robot duo," *IEEE Robotics and Automation Letters*, vol. 7, no. 2, pp. 2132–2139, 2022.

[9] B. Felbrich, M. Prado, S. Saffarian, J. Solly, L. Vasey, J. Knippers, A. Menges, *et al.*, "Multi-machine fabrication: an integrative design process utilising an autonomous uav and industrial robots for the fabrication of long-span composite structures," 2017.

[10] K. Zhang, P. Chermprayong, F. Xiao, D. Tzoumanikas, B. Dams, S. Kay, B. B. Kocer, A. Burns, L. Orr, C. Choi, *et al.*, "Aerial additive manufacturing with multiple autonomous robots," *Nature*, vol. 609, no. 7928, pp. 709–717, 2022.

[11] S. Cutler and K. Petersen, "Leveraging tethers for distributed formation control of simple robots," in *2024 IEEE International Conference on Robotics and Automation (Accepted to)*. IEEE, 2024.

[12] L. Fagiano, "Systems of tethered multicopters: modeling and control design," *IFAC-PapersOnLine*, vol. 50, no. 1, pp. 4610–4615, 2017.

[13] M. A. Karimi, V. Alizadehyazdi, B.-P. Busque, H. M. Jaeger, and M. Spenko, "A boundary-constrained swarm robot with granular jamming," in *2020 3rd IEEE International Conference on Soft Robotics (RoboSoft)*. IEEE, 2020, pp. 291–296.

[14] Y.-H. Kim and D. A. Shell, "Bound to help: cooperative manipulation of objects via compliant, unactuated tails," *Autonomous Robots*, vol. 42, no. 8, pp. 1563–1582, 2018.

[15] S. Bhattacharya, S. Kim, H. Heidarsson, G. S. Sukhatme, and V. Kumar, "A topological approach to using cables to separate and manipulate sets of objects," *The International Journal of Robotics Research*, vol. 34, no. 6, pp. 799–815, 2015.

[16] P. Cheng, J. Fink, V. Kumar, and J.-S. Pang, "Cooperative towing with multiple robots," 2009.

[17] S. Eeckhout, M. Nicotra, R. Naldi, and E. Garone, "Nonlinear control of an actuated tethered airfoil," in *22nd Mediterranean Conference on Control and Automation*. IEEE, 2014, pp. 1412–1417.

[18] S. A. Barogh and H. Werner, "Cascaded formation control using angle and distance between agents with orientation control (part 1)," in *2016 UKACC 11th International Conference on Control (CONTROL)*. IEEE, 2016, pp. 1–6.

[19] Y. Liu, J. Liu, Z. He, Z. Li, Q. Zhang, and Z. Ding, "A survey of multi-agent systems on distributed formation control," *Unmanned Systems*, pp. 1–14, 2023.

[20] S. Lupashin and R. D'Andrea, "Stabilization of a flying vehicle on a taut tether using inertial sensing," in *2013 IEEE/RSJ International Conference on Intelligent Robots and Systems*. IEEE, 2013, pp. 2432–2438.

[21] X. Xiao, Y. Fan, J. Dufek, and R. Murphy, "Indoor uav localization using a tether," in *2018 IEEE International Symposium on Safety, Security, and Rescue Robotics (SSRR)*. IEEE, 2018, pp. 1–6.